

Article

Optimization Analysis of Locomotive Diesel Engine Intake System Based on Matlab-Simulink and GT-Power

Feng Jiang ^{1,2}, Wentong Cao ¹, Xueyou Tan ¹, Jie Hu ^{1,2,*}, Junming Zhou ¹ and Zedan Tan ¹

¹ School of Mechanical and Automotive, Guangxi University of Science and Technology, Liuzhou 545006, China; 100001086@gxust.edu.cn (F.J.); cao12580159@163.com (W.C.); tanxueyou123@163.com (X.T.); a13078027926@163.com (J.Z.); 17754551926@163.com (Z.T.)

² Guangxi Key Laboratory of Automobile Components and Vehicle Technology, Guangxi University of Science and Technology, Liuzhou 545006, China

* Correspondence: 100001078@gxust.edu.cn

Abstract: In this paper, based on the coupling calculation of Simulink software and GT-Power software, an Optimizer model method was proposed for a 16V265H diesel engine to study the effects of different ratios of biodiesel (B0, B10, and B20) on the performance of a 16V265H diesel engine at 1000 rpm and 75% load. Firstly, the four parameters of diesel engine power, BSFC, soot emission, and NO_x emission were taken as the result variables of the optimization model. Taking the intake and exhaust timing of the diesel engine as the independent variable of the optimization model, the maximum power, minimum BSFC, and minimum diesel engine emission were studied and analyzed. Finally, the performance parameters were comprehensively analyzed to determine the best intake and exhaust valve timing. Moreover, based on the model optimization, the diesel engine's BSFC and power performance were compared, and the optimal intake timing scheme for the diesel engine with different biodiesel ratios at 75% operating conditions was obtained. The results showed that the maximum power, optimum BSFC, and minimum emissions of the 16V265H diesel engine with different ratios of biodiesel and different intake valve timing angles were also different. Under 75% load conditions, the BSFC reduction rate was up to 6.32%, and the power increase rate was up to 5.87%. In addition, by optimizing the model with B10 biodiesel and the intake valve timing close to 202°CA and the exhaust valve timing close to 98°CA, the diesel engine had the lowest NO_x emission; with B10 biodiesel and the intake timing at 180°CA, the diesel engine had the lowest BSFC; and with B10 biodiesel and the intake valve timing close to 179.5°CA, the diesel engine had the maximum power. In conclusion, the diesel engine is best with B10 biodiesel. This research method can provide a reference for implementing variable intake system technology for the 16V265H diesel engine.

Keywords: optimizer model method; locomotive diesel engine; performance; emission



Citation: Jiang, F.; Cao, W.; Tan, X.; Hu, J.; Zhou, J.; Tan, Z. Optimization Analysis of Locomotive Diesel Engine Intake System Based on Matlab-Simulink and GT-Power. *Processes* **2022**, *10*, 157. <https://doi.org/10.3390/pr10010157>

Academic Editor: Jiaqiang E

Received: 27 December 2021

Accepted: 11 January 2022

Published: 13 January 2022

Publisher's Note: MDPI stays neutral with regard to jurisdictional claims in published maps and institutional affiliations.



Copyright: © 2022 by the authors. Licensee MDPI, Basel, Switzerland. This article is an open access article distributed under the terms and conditions of the Creative Commons Attribution (CC BY) license (<https://creativecommons.org/licenses/by/4.0/>).

1. Introduction

In recent years, with the rapid development of rail transit equipment worldwide [1] the requirements for a high-speed and heavy-load of railway freight are higher and higher [2,3]. In order to meet the market demand, the American EMD company has produced a 6000 HP HXN3 diesel locomotive [4]. The locomotive adopts the world's most advanced 16V265H low emission four-stroke diesel engine. After years of technical renewal and development, the diesel engine has realized quantitative production [5]. The innovative use of biodiesel in a high-power locomotive diesel engine is a cutting-edge technology to deal with the world's energy shortage [6] and increasingly stringent emission regulations [7], and to improve the operational performance of locomotive diesel engines, which helps to improve the emission [8], economy [9], and power performance of locomotive diesel engines [10].

The structural parameters and design parameters of diesel engines, such as cylinder diameter, piston stroke, compression ratio, fuel injection system parameters, valve phase value, and intake and exhaust system parameters [11,12] have a significant impact on the

power, economy, and emission of a diesel engine [13]. Whether a diesel engine or gasoline engine, the structure and in-cylinder working process are extremely complex and changeable thermodynamic reaction processes, and fuel mixture combustion is accompanied by many physical and chemical reactions [14].

Improving the performance of automotive internal combustion engines is the most demanding factor in the development of new engines [15]. The design of intake and exhaust systems can improve volumetric efficiency, so as to provide better torque and horsepower at specific engine speeds, which is necessary [16]. Many experts and scholars have conducted a lot of research and put forward many new technologies to improve engine combustion [17–19]. Therefore, when developing new technologies [20,21], it has become a challenge to improve the performance of automotive internal combustion engines, decide to use fuel better [22], and even seek the actual performance of such engines under transient and steady-state conditions [23].

In recent years, many researchers have engaged in the optimization analysis of engine intake systems. For example, Yang et al. [24] developed the GT-Power model of an engine intake system and analyzed the influence of harmonics on the intake system. In addition, the intake system was optimized by the response surface method. Qi et al. [25] developed a CFD model using Kiva and STAR-CD software to analyze the temperature, concentration, and flow field in the engine cylinder. Then, the intake system was optimized according to the relationship between intake system structure and cylinder flow. Similarly, Pai et al. [26] established the engine simulation model by using GT-power and STAR-CD software, and studied the influence of the intake system on engine performance. The results showed that the engine performance had been significantly improved. In addition, Silva et al. [27] established an engine simulation model using the GT-power model. The relationship between intake manifold volumetric efficiency and geometric parameters was analyzed by the Brent method and the intake system was optimized.

The application of computer simulation technology has dramatically improved and improved the research and development (R&D) and optimization of the traditional internal combustion engine, and the working process of the engine is modelled by simulation software, which can effectively predict the performance of the engine under different working conditions [28]. In order to improve the economic and environmental performance of diesel engines, many researchers have optimized and analyzed the engine intake system in recent years. For instance, Leahu et al. [29] proposed to drive a composite vehicle, running through a DC motor instead of a supercharged engine, to form a composite driven supercharged diesel engine. Depending on the speed and load of the diesel engine, the speed of the motor could be modified by an electronic management system to optimize the air intake system. Wang et al. [30] optimized the intake system by studying the synergistic effects of the fuel injection system, intake system, and combustion system on the combustion characteristics of a controlled intake cyclone diesel engine. Ma et al. [31] studied the effect of intake air temperature on intake efficiency and found that the intake losses decreased significantly with increasing intake air temperature; thus, the increase in intake air temperature helped improve intake air efficiency. Kang et al. [32] used a diesel particulate filter with intake and exhaust throttling to increase the piston pumping, thus optimizing the intake system. Similarly, Cheng et al. [33] widely installed variable geometry turbochargers and exhaust gas recirculation valves on diesel engines to optimize intake airflow control and exhaust gas recirculation ratio. Li et al. [34] investigated smart charge compression ignition, a new dual-fuel combustion mode, by optimizing the intake pressure and thus the intake system. The decrease in exhaust pressure and the rapid increase in intake pressure leads to a pressure difference on the circulating valve. Therefore, Song et al. [35] investigated the auxiliary pressurization technology and determined that there is a trade-off between exhaust and intake to optimize the intake system. Zhen et al. [36] developed a simulation model of a four-cylinder ignition methanol engine using one-dimensional simulation software to study the effects of throttle opening at 30%, 50%, and 70% on engine performance, combustion, and emissions to find the optimal throttle

opening for optimization of the intake system. In addition, Arnau et al. [37] developed a one-dimensional gas dynamics engine model to simulate several variable exhaust valve driving strategies, which provided the best trade-off between exhaust temperature increase and BSFC by using a variable valve assembly strategy for advanced exhaust (early exhaust valve opening and early exhaust valve closing) and delayed intake (late intake valve opening and late intake valve closing) to optimize the diesel engine intake system.

As mentioned earlier, the numerical simulation of internal combustion engine has obvious advantages. Through the detailed mathematical framework, it is considered to be a very effective tool to save experimental costs [38,39]. In this paper, a novel optimization model is used to simulate the intake combustion process. Based on the optimization model, the timing performance index of the intake valve is calculated and compared [40,41]. This paper mainly studies that a 16V265H diesel engine burns three different ratios of biodiesel B0, B10 and B20 at 1000 rpm and 75% load. The parameters such as diesel engine power, BSFC, soot emission and NO_x emission are taken as the result variables of the model. The intake timings of the diesel engine (including intake valve opening (IVO), intake valve closing (IVC), exhaust valve opening (EVO) and exhaust valve closing (EVC)) are taken as the independent variables of the optimization model to determine the optimal valve timing of a 16V265H diesel engine at 1000 rpm and under 75% load condition.

2. Numerical Approaches

The working process of the diesel engine in-cylinder includes complex and integrated processes such as heat transfer, flow, physics, and chemistry. Its basic differential equation is one of the most fundamental equations in simulation calculation [42]. In addition, in diesel engine engineering technology, optimization technology plays a very important role and significance in the process of diesel engine development decision making [43].

2.1. Theory of Diesel Engine Working Process

The core equation of the diesel engine working process simulation software GT-Power module involved in this paper is the basic differential equation of the working process in the cylinder, which is extended to the calculation of combustion, emission, and other models [44]. At the same time, the calculation results of the basic differential equation are used to determine whether the flow coefficient and pressure coefficient of the diesel engine converge.

The combustion and heat transfer processes of the cylinder follow certain rules. The basic equations of the working process of the cylinder are as follows:

(1) Energy conservation equation:

The first law of thermodynamics leads to the following equation:

$$\frac{dU}{d\varphi} = \frac{dQ_B}{d\varphi} + \frac{dm_s}{d\varphi} h_s - \frac{dm_e}{d\varphi} h_e - \frac{dQ_w}{d\varphi} - p \frac{dV}{d\varphi} \quad (1)$$

where U is the internal energy of the system, J; Q_B is the heat energy released by the combustion of fuel in the cylinder, J; Q_w is the heat energy exchanged through the interfaces of the cylinder system, J; h_s and h_e are the specific enthalpies of working medium at intake valve and exhaust valve, J; m_s and m_e is the mass of working medium at intake valve and exhaust valve, kg, p is the working medium pressure in the cylinder, Pa; φ is the crank angle, °; and V is the working volume of the cylinder, m³.

(2) Mass conservation equation:

$$\frac{dm}{d\varphi} = \frac{dm_s}{d\varphi} + \frac{dm_e}{d\varphi} + \frac{dm_B}{d\varphi} \quad (2)$$

where m is the mass of fuel in the cylinder, g; m_B is the instantaneous mass of fuel injected into the cylinder, g.

(3) Equation of state of an ideal gas:

$$pV = mRT \quad (3)$$

where T is the working temperature in the cylinder, K; and R is the gas constant.

2.2. Theoretical Basis of Optimization Methods for Diesel Engine Applications

In this paper, through the Simulink module of Matlab software, the optimization objective function and constraints were given, the optimization model was established, and coupled with GT-Power software to form an innovative Optimizer model for the related optimization design.

The Optimizer optimization model's objective function is set as a real-time variable (RLT variable) that changes with the design variable. By selecting an appropriate iterative method, a series of optimization design vector sequences are generated to obtain objective function value sequences. When the objective function value sequences converge, the sequences eventually tend to the optimal solution. The optimization model optimizer formed by two simulation software usually has two optimization algorithms, namely, the discrete grid method or Brent search method, which can solve this kind of optimization problem [45].

In order to facilitate the study of the optimization method, taking the power of a 16V265H diesel engine as an example, under the premise of determining other parameters, P_e can be expressed as a function of the intake and exhaust valve timing angle φ_B, φ_C . The research shows that the power also changes with intake and exhaust valve timing angle. In order to obtain better power, the optimization mathematical model can be written as follows:

$$\begin{aligned} \min \quad & P_e = f_1(x), x = [\varphi_B, \varphi_C]^T \\ \text{st.} \quad & 149.5 \leq x(1) \leq 269.5 \\ & 76 \leq x(2) \leq 196 \end{aligned} \quad (4)$$

The optimization objective function in Equation (4) is generally difficult to obtain directly. When the diesel engine speed is determined, it is easy to obtain the two-dimensional contour map (i.e., the level set of binary function) between the objective function and the optimization variable under discrete variables by using GT-Power software. Similarly, the mathematical model of BSFC and emission can be obtained.

According to the optimization theory, given the initial search point x_0 , it is not difficult to determine that its negative gradient direction is the direction in which the function value decreases the fastest, so it is determined that the new search point is:

$$x_1 = x_0 - \alpha_0 \nabla f_1(x_0) \quad (5)$$

When the positive real number α_0 takes different values, the new search points will be different, and the function values will be different. As shown in Figure 1, the function values of $x_1^{(0)}$ and $x_1^{(1)}$ obtained at different α_0^0 and α_0^1 are different. At this time, the value of $f_1(x_1)$ changes with variable α_0 , that is, $f_1(x_1) = \psi_1(\alpha_0)$. In order to obtain the minimum value of $f_1(x)$, it is necessary to take the extreme value of all function values, namely:

$$\frac{\partial \psi_1(\alpha_0)}{\partial \alpha_0} = g(\alpha_0) = 0 \quad (6)$$

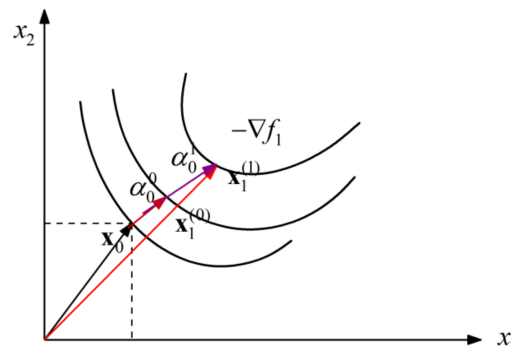


Figure 1. Schematic diagram of one-dimensional search method.

In order to obtain the solution of Equation (6), GT-Power usually uses the Brent method [27] to determine the value of α_0 .

As shown in Figure 1, the Brent method is a faster search method combining dichotomy, linear interpolation, and inverse quadratic interpolation. Its specific operations are as follows:

Firstly, the initialization interval $[a_0, b_0]$ of α_0 is given so that $g(a_0) \cdot g(b_0) < 0$. The estimated value of the iterative root in step k is recorded as $\alpha_0^k = b_k$ (if $|g(a_k)| < |g(b_k)|$, $\alpha_0^k = a_k$), and the estimated values of the iterative roots in the first two steps are recorded as b_{k-1} and b_{k-2} , respectively. Judge whether the following four inequalities are true:

$$|\delta| < |b_k - b_{k-1}| \tag{7}$$

$$|\delta| < |b_{k-1} - b_{k-2}| \tag{8}$$

$$|s - b_k| < \frac{1}{2}|b_k - b_{k-1}|, s = a_k \text{ or } b_k \tag{9}$$

$$|s - b_k| < \frac{1}{2}|b_{k-1} - b_{k-2}| \tag{10}$$

Judge whether any one of the following five conditions are true:

- (1) The k -1st iteration is dichotomous and (7) does not hold;
- (2) The k -1st iteration is dichotomous and (8) does not hold;
- (3) The k -1st iteration is an interpolation and (9) does not hold;
- (4) The k -1st iteration is an interpolation and (10) does not hold;
1. The temporary value s calculated by the interpolation method is not in the interval $[\frac{3a_k + b_k}{4}, b_k]$.

If yes, the iterative value α_0^{k+1} of the current root is obtained by dichotomy:

$$\alpha_0^{k+1} = \frac{1}{2}(a_k + b_k) \tag{11}$$

Otherwise, judge whether the following formula is true:

$$\alpha_0^{k-1} \neq \alpha_0^k, \alpha_0^{k-1} \neq \alpha_0^{k+1}, \alpha_0^k \neq \alpha_0^{k+1} \tag{12}$$

If Equation (12) holds, then

$$\begin{aligned} \alpha_0^{k+1} &= \frac{g(\alpha_0^{k-1})g(\alpha_0^k)}{(g(\alpha_0^{k-2}) - g(\alpha_0^{k-1}))(g(\alpha_0^{k-2}) - g(\alpha_0^k))} \alpha_0^{k-2} \\ &+ \frac{g(\alpha_0^{k-2})g(\alpha_0^{k-1})}{(g(\alpha_0^k) - g(\alpha_0^{k-2}))(g(\alpha_0^k) - g(\alpha_0^{k-1}))} \alpha_0^k \\ &+ \frac{g(\alpha_0^{k-2})g(\alpha_0^k)}{(g(\alpha_0^{k-1}) - g(\alpha_0^{k-2}))(g(\alpha_0^{k-1}) - g(\alpha_0^k))} \alpha_0^{k-1} \end{aligned} \tag{13}$$

If Equation (12) does not hold, then

$$\alpha_0^{k+1} = b_k - \frac{(b_k - a_k)g(b_k)}{g(b_k) - g(a_k)} \quad (14)$$

It should be noted that for the temporary value $s = \alpha_0^{k+1}$ in the above Equations (9) and (10), after each iteration, the interval $[a_k, b_k]$ of the root will be further reduced to $[a_{k+1}, b_{k+1}]$, where $a_{k+1} = s$ or $b_{k+1} = s$, and the other endpoint is one of a_k and b_k , and the following conditions are met:

$$g(a_{k+1}) \cdot g(b_{k+1}) < 0, \text{ and } |g(a_{k+1})| > |g(b_{k+1})| \quad (15)$$

Repeat the above iteration until α_0 converges, that is, the interval length of the solution tends to an infinitesimal value.

$$|a_{k+1} - b_{k+1}| \leq \varepsilon_1 \quad (16)$$

By analogy, it is not difficult to construct the iterative point sequence as follows:

$$x_{k+1} = x_k - \alpha_k \nabla f_1(x_k), \quad (k = 1, 2, \dots) \quad (17)$$

In addition, in each iteration step, the positive real number α_k can be determined according to the following equation:

$$\frac{\partial \psi_1(\alpha_k)}{\partial \alpha_k} = 0 \quad (18)$$

Until the sequence satisfies the following convergence conditions:

$$\|x_{k+1} - x_k\| \leq \varepsilon \quad (19)$$

In Equation (19), $\|\cdot\|$ is the norm of the vector and ε is a minimal positive real value.

In the subsequent optimization calculation in this paper, because the design variables are two (intake and exhaust timing angles), the problem can be expressed as a constrained optimization problem and the Brent method can be used for optimization design. At the same time, according to the design variables generated by each iteration data and their corresponding objective function values, the contour map (i.e., cloud map type) of the objective function varying with the design variables will be generated to present the optimization design process in a more intuitive form.

2.3. Optimizer Model

As an optimization model, when the optimization result variable is the maximum or minimum value, its change needs to meet the following trend: the result variable first increases to the maximum value and then decreases, or decreases to the minimum value and then increases (i.e., the only maximum or minimum value) with the independent variable (giving the initial value, setting the independent variable range and step accuracy). The optimization result variable is shown in Figure 2.

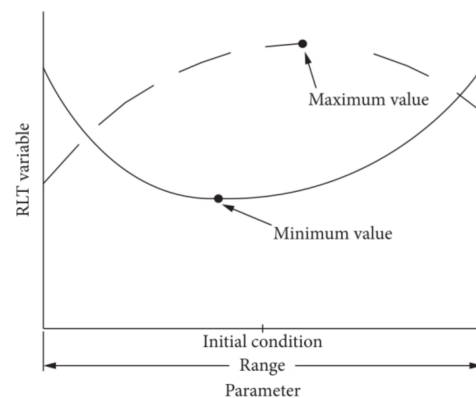


Figure 2. Optimizer model.

It can be seen from Figure 2 that the Optimizer model works by running the calculation until it reaches a stable state (one iteration), then resetting one or more parameters and running again until the optimal value is found. This structural feature can obtain stable iterative calculation. The optimizer optimization model is coupled with GT-Power software through the Matlab software Simulink module. After debugging and running Simulink, the GT-Power is mobilized to the optimized algorithm.

It can be seen from the changing trend in Figure 2 that the parameters including power, torque, BSFC, emission and inflation efficiency in each performance index of the internal combustion engine can be used as the result variables of the Optimizer optimization model, while the independent variable parameters including intake and exhaust timing, throttle opening, and important structural parameters can be used as the independent variables of the Optimizer optimization model. At present, the author is optimizing the valve timing of a gasoline engine under various working conditions based on the Optimizer model and taking the inflation efficiency as the optimization objective, so as to determine the optimal valve timing angle at various speeds and improve the engine performance to a certain extent.

2.4. Fuel Properties

The typical biodiesels are mainly composed of five components, methyl linolenate (C18:3), methyl linoleate (C18:2), methyl oleate (C18:1), methyl stearate (C18:0), and methyl palmitate (C16:0). Cm:n is the shorthand of fatty acid methyl esters (FAME), n is the number of double bonds, and m is the number of carbon atoms. It is generally believed that the major components of typical biodiesels are also the above five components, and other components such as C12:0, C14:0, and C20:0 can be ignored. Soybean oil methyl ester (SME) was obtained from soybean oil and methanol by transesterification. The transesterification of soybean oil was carried out under the catalysis of alkali, and the reaction time was about 1 h. The molar ratio of methanol to oil is 6:1, and the alkali catalyst is 1% wt/wt KOH. Based on the fatty acid profile, the SME properties were analyzed by “Biodiesel Analyzer”. The main instruments and test standards for physical and chemical property tests are shown in Table 1. In the paper, an Agilent 7890 N GC-MS analyzer was used for measuring the composition of fatty acids of biodiesel. Table 2 shows the fatty acid profile of biodiesel [10,46–48]. In addition, the kinematic viscosity of biodiesel is measured according to ASTM D445. Similarly, the lower calorific value of biodiesel is measured according to ASTM D240.

Table 1. Main instruments and test standards.

Physical and Chemical Parameters	Test Instrument	Test Standard	Accuracy
Kinetic viscosity (mm ² /s) (at 40 °C)	SYD-265H	GB/T265	±0.05%
Density (g/cm ³)	KD-R1022	ADTM D445	±0.1%
Calorific value (MJ/kg)	MTZW-A4	ASTM D240	±0.1%
Surface tension (mN/m)	JYW-200	GB/T6541-86	≤±1%FS

Table 2. Physical properties of FAMES present.

Type	Kinetic Viscosity (mm ² /s) (at 40 °C)	Density (g/cm ³)	Molecular Weight (g/mol)	Higher Calorific Value (MJ/kg)	SME Composition % Volume
C18:3	3.11	0.899	292	39.43	8.11
C18:2	3.79	0.887	294	39.68	22.27
C18:1	4.60	0.875	296	39.93	65.18
C18:0	5.59	0.863	298	40.18	0.87
C16:0	4.37	0.864	270	39.56	3.57

The biodiesel made from 0# diesel and soybean “wool” oil was blended with 0%, 10%, and 20% volume fractions (recorded as B0, B10, and B20) to determine the compatibility, cold filter point, freezing point, density, cetane number, kinematic viscosity, flash point, etc., respectively. The main experimental equipment is: DYS-006B pour point, cloud point, freezing point, cold filtration point tester; kinematic viscosity determination thermostat bath; BSH-2 closed-end flash tester; DSY-020 copper corrosion turbidity tester for petroleum products; DSS-1 petroleum products moisture tester; and DRD-100 automatic distillation tester, etc. The test results are shown in Table 3.

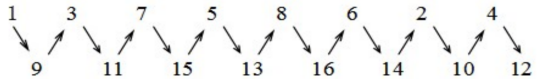
Table 3. The properties of biodiesel with different ratios.

Type	B0	B10	B20
Density (20 °C)/(kg·m ⁻³)	836.3	842.2	850.1
Sulfur content (mass fraction)/%	0.0234	0.0187	0.0143
Acidity/(mgKOH/100 mL)	4.49	3.03	4.19
Copper corrosion (50 °C, 3 h)/grade	≤1	≤1	≤1
Kinematic viscosity (20 °C)/(mm ² ·s ⁻¹)	4.578	8.057	8.627
Flash point (closed) (°C)	63	74	74
Cold filter point (°C)	−4	2	2
Condensation point (°C)	−7	−6	−5
Boiling point (°C)	180~370	142	145
Heptadecane index	54.8	53.5	52.1

2.5. Engine Specifications

The 16V265H diesel engine adopts turbocharging and electronically controlled unit pump fuel injection technology with a rated power of 4660 kw, rated speed of 1000 rpm, and displacement of 264.74 L. The main technical parameters are shown in Table 4. The layout of the diesel engine bench test room is shown in Figure 3. The simulation model of the entire diesel engine is shown in Figure 4.

Table 4. The major technique parameters of the 16V265H diesel engine.

Model	16V265H
Type	Four stroke, direct injection, exhaust gas turbocharging, supercharging, and intercooling
Number of cylinders and V-angle	16 cylinders, 45°
Bore × stroke	265 × 300 mm
Total displacement	264.74 L
Compression ratio	15.4
Calibration power	4660 kW
Calibration speed	1000 rpm
Minimum idle stable speed	325 rpm
Minimum working stable speed	400 rpm
Average piston speed	10 m/s
Firing sequence	
Start mode	Air motor start
Crankshaft steering	Facing the output, counterclockwise
Overall dimensions: long × wide × high	5890 × 1780 × 2760 mm

**Figure 3.** Picture of diesel engine bench test.

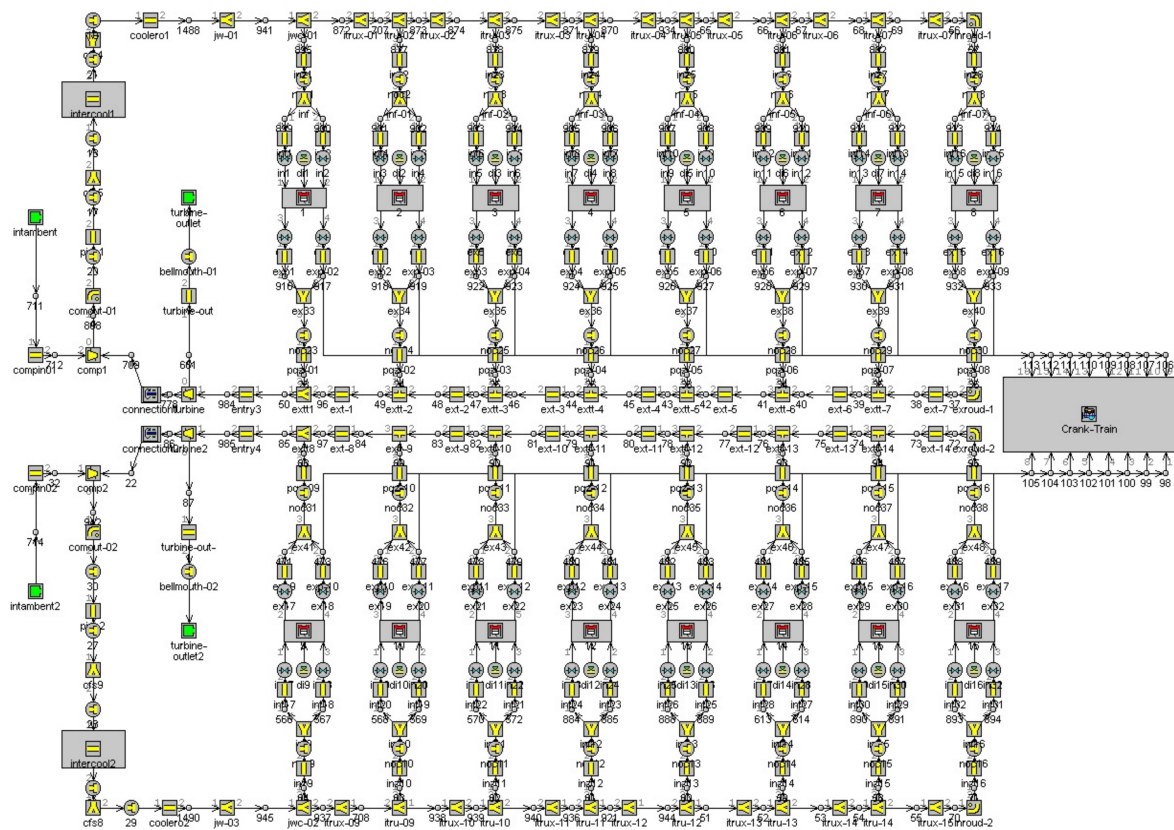


Figure 4. Simulation model of the entire diesel engine.

3. Results and Discussion

Because 1000 rpm and 75% load are the most common operating conditions of the locomotive diesel engine [4], in this paper, biodiesel with different ratios was studied (B0, B10, and B20) on the performance of the 16V265H diesel engine under 75% load condition at 1000 rpm. Firstly, the four parameters of diesel engine power, BSFC, soot emission, and NO_x emission are taken as the result variables of the Optimizer optimization model. The intake and exhaust timings of the diesel engine are taken as the independent variables of the Optimizer optimization model to study and analyze the maximum power, minimum BSFC, and minimum exhaust emission. Finally, the performance parameters are comprehensively analyzed to determine the optimal intake and exhaust valve timing. This research method can provide a reference for a 16V265H diesel engine to realize variable intake system technology.

3.1. Power Optimization Analysis of 16V265H Diesel Engine

Figure 5 shows the optimal calculation results of maximum power generated by a 16V265H diesel engine burning biodiesel with different ratios (B0, B10, and B20) at 1000 rpm and 75% load. As can be seen from the figure, the more concentrated the red area means that the optimization result is closer to the target value, and the more concentrated the distribution of points in the red area means that the area is closer to the optimal target value area.

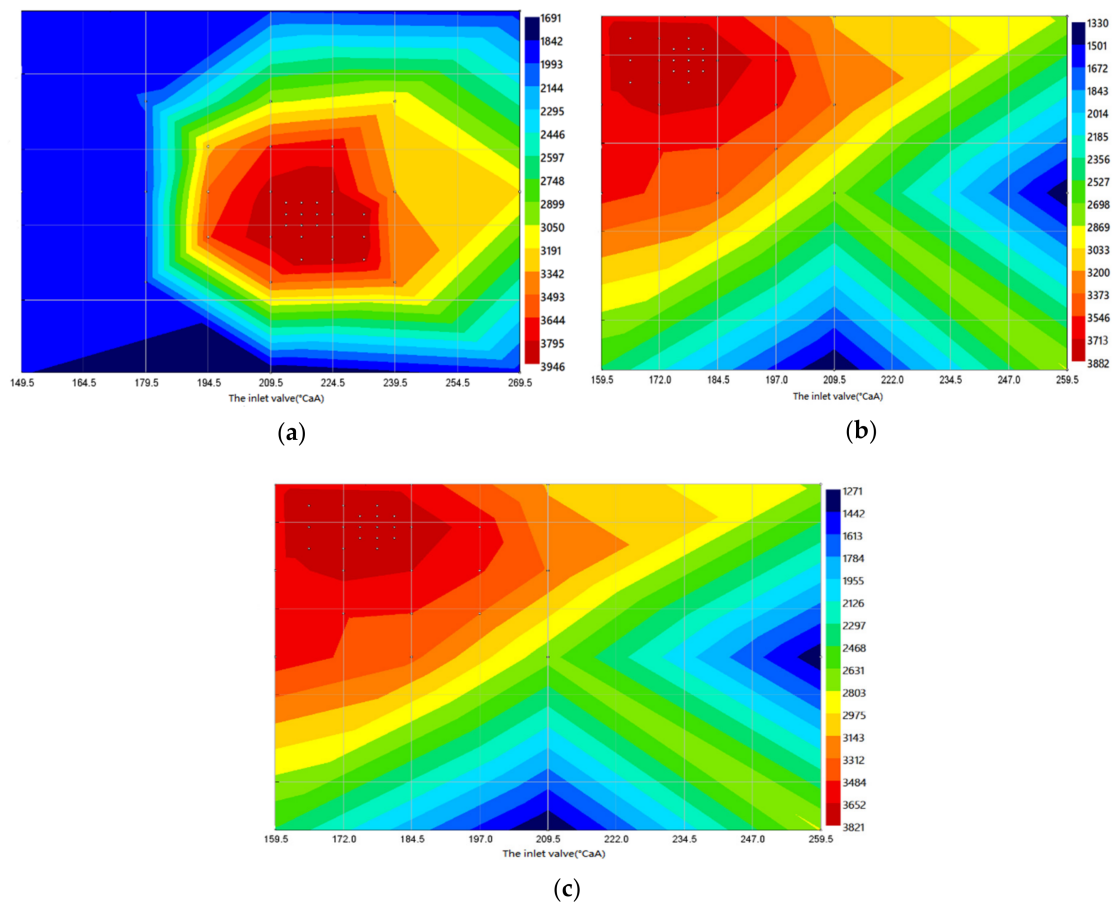


Figure 5. (a) B0, (b) B10, and (c) B20. Power of different biodiesel ratios under 75% load condition.

As can be seen from Figure 5a, the diesel engine is in the combustion of pure diesel B0 and the maximum power region appears around 217°CA at intake valve timing. Judging from the cloud map, as the intake valve timing increases from the minimum range angle of 149.5°CA to 180°CA , the power value changes little; when the intake valve timing angle is greater than 180°CA , the power calculation value is incremented; and when the maximum region is 217°CA , the timing angle continues to increase and the power shows a downward trend. From the color change trend in the cloud diagram, it can be seen that the power value has the maximum value within the optimization calculation range, and it increases first and then decreases with the increase in valve timing angle. The power has a unique maximum target value within a given calculation range, which is in line with the theory of the Optimizer optimization model. Judging from the calculation results, the intake valve closing delay is about 8°CA (that is, the intake valve timing is around 217°CA), and the output power of the diesel engine has a maximum region.

As can be seen from Figure 5b, in the vicinity of intake valve timing from 165°CA to 194.5°CA , the maximum power optimization dense distribution region appears. This is because the valve overlap angle in the valve timing range corresponds to a large amount of intake air flow, the fuel gas mixture in the cylinder is fully mixed and the combustion effect is good, and the power increases accordingly. Judging from the calculation results, the intake valve closing needs to be delayed by about 30°CA (that is, the intake valve timing is near 179.5°CA); the output power of the diesel engine has a maximum area.

As can be seen from Figure 5c, when B20 biodiesel is used, the maximum power region of the diesel engine is around 179.5°CA at the positive valve timing. Judging from the cloud map, extremely low power occurs in two areas near the intake valve timing of 209.5°CA (initial intake valve timing angle) and the intake valve timing of 259.5°CA .

As can be seen from Figure 5, the 16V265H diesel engine uses different ratios of biodiesel (B10, B20) at a speed of 1000 rpm and 75% load. The maximum output power is the optimized target value, and the intake valve is closed about 30°CA in advance (that is, the intake valve timing is around 179.5°CA); the diesel engine has the highest output power. When B0 pure diesel is used, the intake valve closing needs to be delayed by about 8°CA (that is, the intake valve timing is around 217°CA); at this time, the output power of the diesel engine is the maximum.

It can be seen from Figure 6 that the power value of the diesel engine after optimization is higher than the power value before optimization, and when the ratios of biodiesel increase (such as B10 to B20), the power of the diesel engine shows a slightly decreasing trend. The power value of the diesel engine burning B10 and B20 biodiesel is slightly lower than that of B0 pure diesel. Therefore, there is strong practical significance for the use of low-ratio biodiesel (such as: B10, B20).

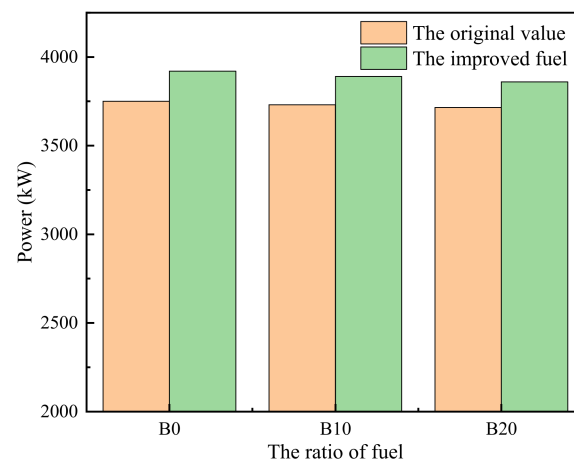


Figure 6. Comparison between the improved power and the original value under 75% load.

It can be seen from Figures 5 and 6 that after optimizing based on the Optimizer model, the output power of the diesel engine fueled with various ratios of biodiesel has been increased, and the output power is higher than the original engine's initial valve timing angle (the initial intake valve timing angle is 209.5°CA) generated power. The optimized diesel engine can greatly improve the oil–gas mixing effect and increase the output power of the diesel engine. The output power of this diesel engine when burning B10 and B20 biodiesel is slightly lower than the output power when burning B0 pure diesel. Based on the optimization results of the Optimizer model, it can be concluded that the optimal solution for the diesel engine to use different ratios of biodiesel under 75% load conditions is: B10 biodiesel with the intake valve timing at 179.5°CA (that is, the intake angle of the early door closing is 30°CA). This scheme can achieve the effect of maximizing the power of burning biodiesel fuel.

3.2. Analysis of Brake Specific Fuel Consumption Optimization of 16V265H Diesel Engine

Figure 7 shows the optimal calculation results of minimum brake specific fuel consumption (BSFC) by a 16V265H diesel engine burning biodiesel with different ratios (B0, B10, and B20) at 1000 rpm and 75% load.

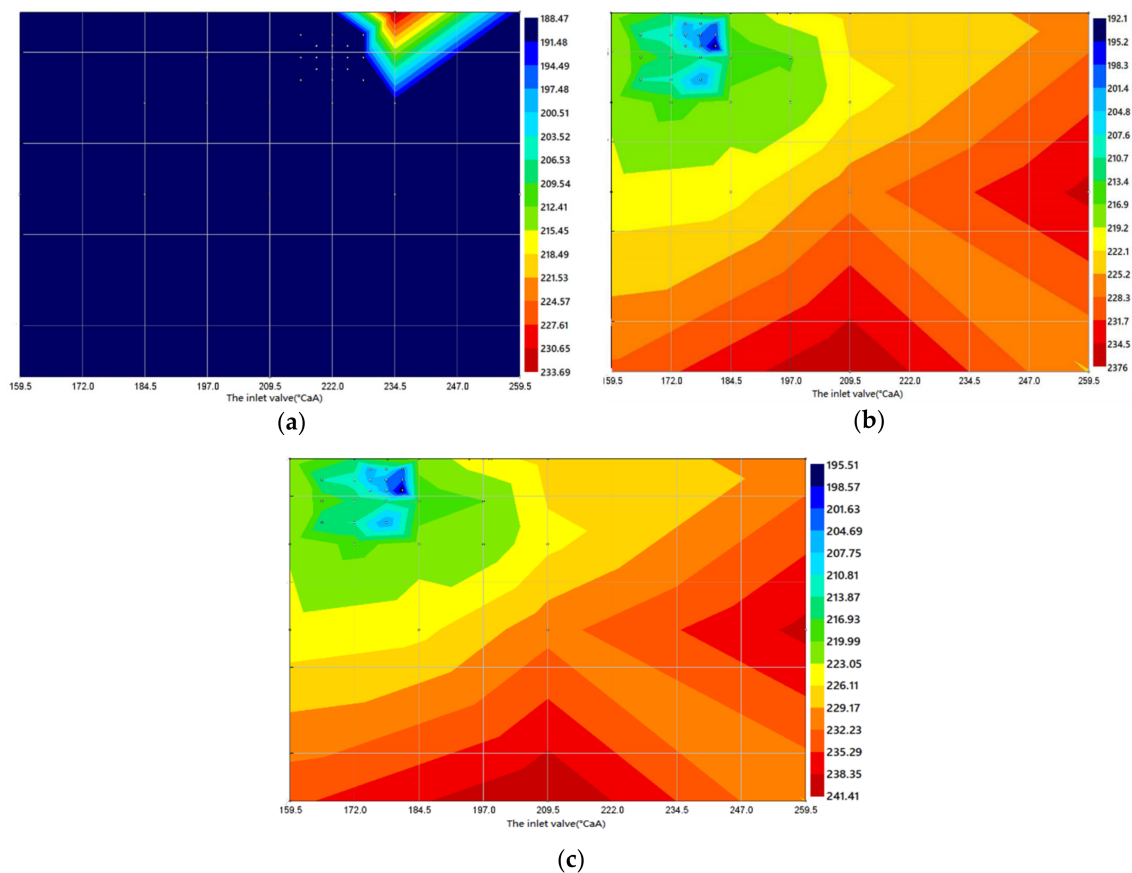


Figure 7. (a) B0, (b) B10, (c) B20. BSFC of different biodiesel ratios under 75% load condition.

As can be seen from Figure 7a, under the condition of B0 pure diesel, the diesel engine has the lowest BSFC near the intake valve timing of 222°CA . It can be seen from Figure 7b,c that the BSFC optimization results of B10 and B20 biodiesel have similar trends. All of them appear near the intake valve timing of 180°CA in a densely distributed small area with the lowest BSFC optimization; the difference between the intake and exhaust valve angles that need to be optimized and adjusted is small.

Based on the three diagrams in Figure 7, it can be concluded that the 16V265H diesel engine uses different ratios of biodiesel (B0, B10, and B20) at a speed of 1000 rpm and 75% load, with the lowest BSFC as the optimal target value. It can be determined that using B10 biodiesel has the best effect, and the closing of the intake valve needs to be delayed by about 29°CA (that is, the intake valve timing is 180°CA attached). This diesel engine has the lowest BSFC. When B0 pure diesel is used, the diesel engine has the lowest BSFC near the intake valve timing of 222°CA .

Figure 8 shows the BSFC optimization comparison of a 16V265H diesel engine at 1000 rpm and 75% load when using three different ratios of biodiesel. It can be seen from the figure that the BSFC of the diesel engine after model optimization is lower than the BSFC before optimization, and when the ratio of biodiesel increases (such as B0 to B10), the BSFC of the diesel engine slightly increases. When using B10 and B20 biodiesel, the diesel engine BSFC is slightly higher than that of pure diesel B0, and the BSFC increases with the increase in the biodiesel ratios. This is because the calorific value of biodiesel is lower than the calorific value of B0 pure diesel. With an output of the same power, the amount of fuel required will increase. After optimization based on the model, the BSFC of diesel engines fueled by biodiesel at various ratios was reduced.

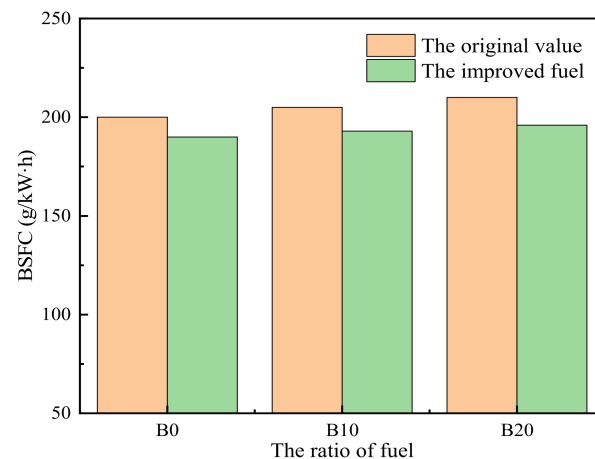


Figure 8. Comparison between the improved BSFC and the original value under 75% load.

According to a comprehensive analysis, the Optimizer model is used to calculate the use of different ratios of biodiesel under 75% load conditions. It is concluded that the optimal solution under this operating condition is: B10 biodiesel is used, and the intake valve closing needs to be delayed by about 29°CA (that is, the intake valve timing is around 180°CA); the diesel engine has the lowest BSFC.

3.3. Optimization Analysis of Soot Emission from 16V265H Diesel Engine

Figure 9 shows the optimal calculation results of soot emission by a 16V265H diesel engine burning biodiesel with different ratios (B0, B10, and B20) at 1000 rpm and 75% load. The more concentrated the red area of the cloud map represents the greater the soot emission value; the denser the blue area and the more concentrated the point distribution represents the closer the area is to the optimal target value area.

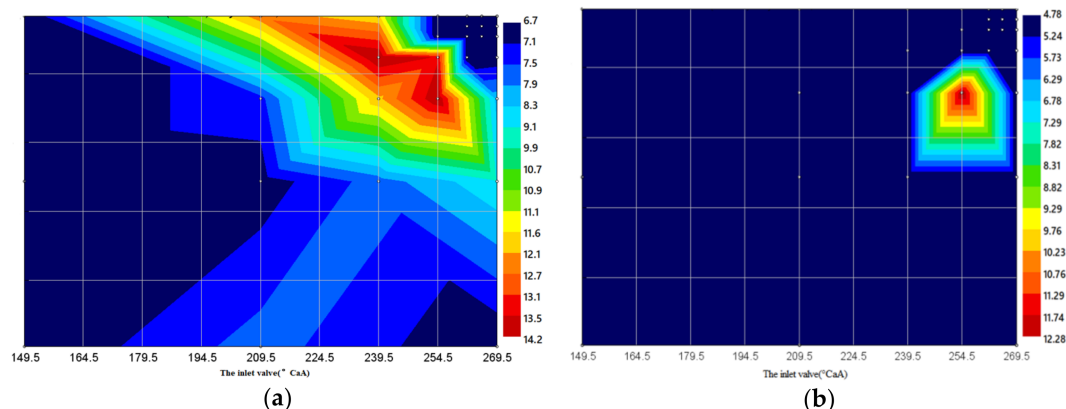


Figure 9. (a) B0 and (b) B20. Soot emission of different biodiesel ratios under 75% load condition.

It can be seen from Figure 9a that when the diesel engine uses pure diesel B0, the highest soot emission occurs in two areas near the intake valve timing of 239.5°CA and the intake valve timing of 254.5°CA . The soot emission is the lowest in the area centered around the intake valve timing of 264.5°CA (the area where the number of points is concentrated).

From Figure 9b, it can be seen from the soot emission optimization results produced when diesel engines use B20 biodiesel (B10 biodiesel optimization results are also similar) that the lowest soot emission is in the area centered around the intake valve timing of 264.5°CA . In the area centered around 254.5°CA at the intake valve timing, the maximum soot emission appears.

Figure 10 shows the soot emission optimization results of a 16V265H diesel engine fueled with different ratios of biodiesel under 1000 rpm and 75% load conditions. It can be

seen from the figure that the optimized soot emission of the diesel engine has decreased significantly; the diesel engine has the lowest soot emission when using B20 pure biodiesel, and when the ratio of biodiesel increases, the soot emission of the diesel engine shows a downward trend. The highest soot emission is when B0 pure diesel is used, which shows that the use of biodiesel has the effect of reducing soot emission.

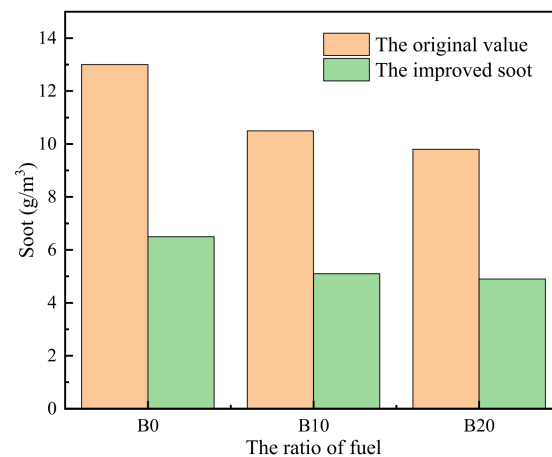


Figure 10. Comparison between the improved soot and the original value under 75% load.

According to the calculation of the 16V265H diesel engine fueling different ratios of biodiesel under the operating condition of 1000 rpm and 75% load through the model, it is concluded that the optimal solution under this operating condition is: when B20 biodiesel is used, the soot emission of the diesel engine is the lowest when the intake valve timing is near 264.5°CA and the exhaust valve timing is near 191°CA. The effect of burning B10 biodiesel is the second optimal solution.

3.4. Optimization Analysis of 16V265H Diesel Engine

Figure 11 shows the optimal calculation results of NO_x emission by 16V265H diesel engine burning B0 at 1000 rpm and 75% load.

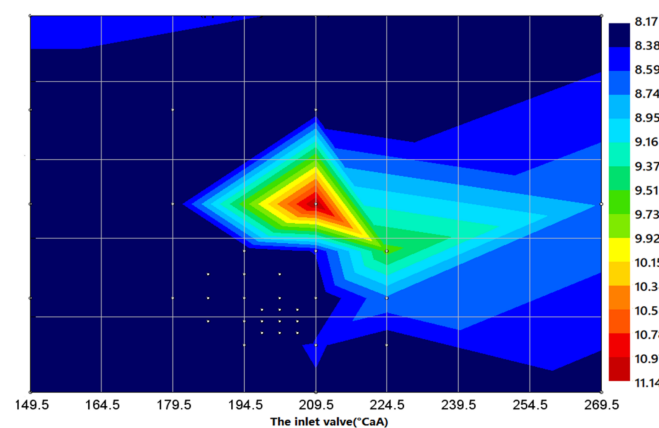


Figure 11. NO_x emission of B0 under 75% load condition.

Figure 11 shows the NO_x emission optimization results of the 16V265H diesel engine burning B0 pure diesel at 1000 rpm and 75% load. It can be seen from the figure that when this diesel engine uses B0 pure diesel, the maximum NO_x emission occurs near the intake valve timing of 209.5°CA. The lowest NO_x emission area appears near the intake valve timing of 202°CA; the trends of other biodiesel ratios (B10, B20) are similar to those of B0.

Figure 12 shows the NO_x emission optimization results of a 16V265H diesel engine fueled with different ratios of biodiesel under 1000 rpm and 75% load conditions. It can be

seen from the figure that the NO_x emission of the diesel engine after model optimization is lower than before optimization. The diesel engine has the lowest NO_x emission when fueled by B0 pure diesel.

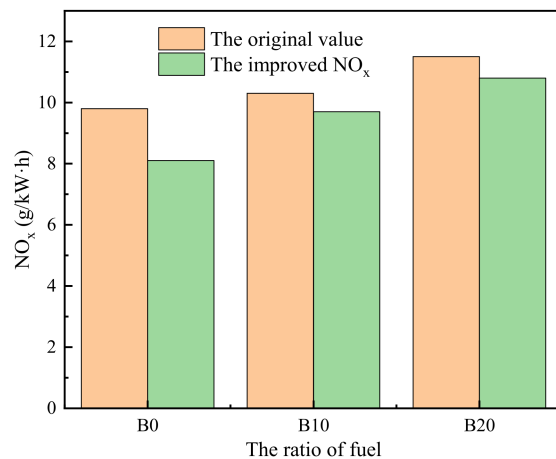


Figure 12. Comparison between the improved NO_x and the original value under 75% load.

The Optimizer model is used to calculate the different ratios of biodiesel used by a 16V265H diesel engine at the speed of 1000 rpm and 75% load. It is concluded that the optimal scheme is as follows: B10 biodiesel fuel, intake valve timing near 202°CA, the exhaust valve timing near 98°CA; NO_x emission of the diesel engine is the lowest. The effect of using B20 biodiesel is the second-best scheme. NO_x emission of diesel engine is related to combustion temperature and oxygen content in the oil–gas mixture during combustion (i.e., high-temperature oxygen enrichment condition) [17,18]. The use of biodiesel makes the injection occur earlier and leads to an increase in NO_x emission; therefore, the more biodiesel content, the more NO_x emission.

3.5. Performance Comparison Based on Model Optimization

According to the optimization results of the various performance parameters of the 16V265H diesel engine by the Optimizer model, it is feasible to use low-ratio biodiesel in locomotive diesel engines. The initial valve timing bench test was compared with the optimized calculated value. The comparison indicators are BSFC and power, as shown in Table 5.

Table 5. The performance comparison before and after biodiesel optimization.

	Oil Consumption (g/(kW·h))			Power (kW)		Improve the Range
	Original Machine Test Value	Optimize Simulation Value	Degree of Declining	Original Machine Test Value	Optimize Simulation Value	
B0	201.2	188.48	6.32%	3751	3971	5.86%
B10	205.18	192.2	6.32%	3691	3908	5.87%
B20	208.77	195.57	6.31%	3631	3844	5.86%

It can be seen from the table that when the diesel engine is optimized, its BSFC has been significantly reduced compared with the original engine, its power has been improved, and the trend of the range optimization effect is relatively consistent. Under 75% load condition, the BSFC reduction rate is up to 6.32% and the power increase rate is up to 5.87%. The diesel engine uses B10 biodiesel under 75% load conditions and has the best effect.

4. Conclusions

Currently, with the rapid developments in economy and industrial automation, the shortage of resources (such as non-renewable energy [49–51], oil [52], and coal [53]) and environmental pollution (air pollution [54–57] and human health [58]) are becoming more and more serious. How to effectively control energy shortages and reduce engine emissions are the main areas of interest for researchers today. In this paper, based on the simulation model of a 16V265H diesel engine built by GT-Power software, the Optimizer optimization model coupled with Simulink and GT-Power was used to study the parameters of diesel engine power, BSFC, and emission as the optimization objectives under different load conditions for diesel engines burning biodiesel with different ratios. The main conclusions obtained are as follows.

(1) The maximum power increase in this diesel engine when fueled with B0 at 75% load condition is 5.9%. The optimal solution for power under 75% load condition is obtained through the Optimizer model optimization: B10 biodiesel fuel, intake valve timing of 179.5°CA near the maximum power. This is because the intake air flow corresponding to the valve overlap angle within the valve timing range is large, the oil–gas mixture in the cylinder is sufficient, the combustion effect is good, and the power increases accordingly.

(2) The BSFC of the diesel engine under 75% load condition is reduced after optimization. Through the Optimizer model optimization, the optimal BSFC scheme under 75% load conditions is: use B10 biodiesel with the intake valve timing at 180°CA; this scheme has the lowest BSFC. The main reason is that the intake air corresponding to the valve overlap angle near the valve timing increases, resulting in full fuel blending, more complete combustion, and reduced fuel consumption.

(3) Based on the Optimizer model optimization, the soot emission of this diesel engine under 75% load conditions with different ratios of biodiesel decreases as the ratio increases, and the lowest carbon smoke emission is achieved when B20 biodiesel is used. From the optimization results, it can be seen that the optimal solution for the diesel engine to reduce soot emission under 75% load conditions with different ratios of biodiesel is: using B20 biodiesel with soot of the diesel engine near 264.5°CA at the intake valve timing, the emission is the lowest; the effect of using B10 biodiesel is the second optimal scheme.

(4) Based on the Optimizer model optimization, the diesel engine burning different ratios of biodiesel under 75% load condition shows an increasing trend of NO_x emission with the increase in the ratio. With the increase in the injection advance angle and the extension of the ignition delay period, the amount of fuel injected into the cylinder in the premixing stage increases. A large amount of oil–gas mixture burns instantaneously in the premixing stage, releasing a large amount of heat; the temperature and pressure in the cylinder rise sharply, and the NO_x emission increases. From the optimization results, it can be seen that the optimal solution for this diesel engine to use different ratios of biodiesel to reduce NO_x emission at 75% load is: the intake valve timing is near 202°CA and B10 biodiesel is used.

Author Contributions: Conceptualization, F.J.; software, F.J., W.C.; formal analysis, F.J., J.H. and Z.T.; investigation, F.J., W.C., X.T., J.H., J.Z. and Z.T.; resources, F.J.; writing—original draft preparation, F.J., W.C., J.H.; writing—review and editing, F.J., W.C., X.T., J.H., J.Z. and Z.T.; supervision, F.J.; funding acquisition, F.J., X.T., J.H. All authors have read and agreed to the published version of the manuscript.

Funding: This research was funded by the Doctoral Fund Project of Guangxi University of Science and Technology, grant number 21Z34 and 21Z46.

Institutional Review Board Statement: Not applicable.

Data Availability Statement: All data used to support the findings of this study are included within the article.

Acknowledgments: This research was funded by the Doctoral Fund Project of Guangxi University of Science and Technology, grant number 21Z34 and 21Z46.

Conflicts of Interest: The authors declare that there is no conflict of interest regarding the publication of this paper.

Nomenclature

CACO	Crankshaft angle	Carbon monoxide
HC	Hydrocarbon	
NO _x	Nitrogen oxides	
CO ₂	Carbon dioxide	
PM	Particulate matter	
CFD	Computational fluid dynamics	
NO ₂	Nitrogen dioxide	
NO	Nitric oxide	
BSFC	Brake specific fuel consumption	
BTE	Brake thermal efficiency	
NG	Natural gas	
RCCI	Reactivity controlled compression ignition	
LCV	Low calorific value	
SOI	Start of injection	
ECU	Electronic control unit	
IVO	Intake valve opening	
IVC	Intake valve closing	
EVO	Exhaust valve opening	
EVC	Exhaust valve closing	
FAME	Fatty acid methyl esters	
SME	Soybean oil methyl ester	
B0	100% diesel + 0% biodiesel	
B10	90% diesel + 10% biodiesel	
B20	80% diesel + 20% biodiesel	

References

- Jiaqiang, E.; Zhang, Z.; Chen, J.; Pham, M.; Zhao, X.; Peng, Q.; Zhang, B.; Yin, Z. Performance and emission evaluation of a marine diesel engine fueled by water biodiesel-diesel emulsion blends with a fuel additive of a cerium oxide nanoparticle. *Energy Convers. Manag.* **2018**, *169*, 194–205. [[CrossRef](#)]
- Cai, T.; Zhao, D.; Wang, B.; Li, J.; Guan, Y. NO emission and thermal performances studies on premixed ammonia-oxygen combustion in a CO₂-free micro-planar combustor. *Fuel* **2021**, *280*, 118554. [[CrossRef](#)]
- Peng, Q.; Xie, B.; Yang, W.; Tang, S.; Li, Z.; Zhou, P.; Luo, N. Effects of porosity and multilayers of porous medium on the hydrogen-fueled combustion and micro-thermophotovoltaic. *Renew. Energy* **2021**, *174*, 391–402. [[CrossRef](#)]
- Xie, B.; Peng, Q.; Yang, W.; Li, S.; E, J.; Li, Z.; Tao, M.; Zhang, A. Effect of pins and exit-step on thermal performance and energy efficiency of hydrogen-fueled combustion for micro-thermophotovoltaic. *Energy* **2022**, *239*, 122341. [[CrossRef](#)]
- Cai, T.; Zhao, D. Mitigating NO_x emissions from an ammonia-fueled micro-power system with a perforated plate implemented. *J. Hazard. Mater.* **2021**, *401*, 123848. [[CrossRef](#)] [[PubMed](#)]
- Zhang, Z.; Ye, J.; Tan, D.; Feng, Z.; Luo, J.; Tan, Y.; Huang, Y. The effects of Fe₂O₃ based DOC and SCR catalyst on the combustion and emission characteristics of a diesel engine fueled with biodiesel. *Fuel* **2021**, *290*, 120039. [[CrossRef](#)]
- Tan, D.; Chen, Z.; Li, J.; Luo, J.; Yang, D.; Cui, S.; Zhang, Z. Effects of Swirl and Boiling Heat Transfer on the Performance Enhancement and Emission Reduction for a Medium Diesel Engine Fueled with Biodiesel. *Processes* **2021**, *9*, 568. [[CrossRef](#)]
- Fan, L.; Cheng, F.; Zhang, T.; Liu, G.; Yuan, J.; Mao, P. Visible-light photoredox-promoted desilylative allylation of *α*-silylamines: An efficient route to synthesis of homoallylic amines. *Tetrahedron Lett.* **2021**, *81*, 153357. [[CrossRef](#)]
- Cai, T.; Becker Sid, M.; Cao, F.; Bing Wang, B.; Tang, A.; Fu, J.; Han, L.; Sun, Y.; Zhao, D. NO_x emission performance assessment on a perforated plate-implemented premixed ammonia-oxygen micro-combustion system. *Chem. Eng. J.* **2021**, *417*, 128033. [[CrossRef](#)]
- Zhang, Z.; E, J.; Chen, J.; Zhu, H.; Zhao, X.; Han, D.; Zuo, W.; Peng, Q.; Gong, J.; Yin, Z. Effects of low-level water addition on spray, combustion and emission characteristics of a medium speed diesel engine fueled with biodiesel fuel. *Fuel* **2019**, *239*, 245–262. [[CrossRef](#)]
- Poorghasemi, K.; Saray, R.; Ansari, E.; Irdmousa, B.; Shahbakhti, M.; Naber, J. Effect of diesel injection strategies on natural gas/diesel RCCI combustion characteristics in a light duty diesel engine. *Appl. Energy* **2017**, *199*, 430–446. [[CrossRef](#)]
- Zhang, Z.; Tian, J.; Li, J.; Ji, H.; Tan, D.; Luo, J.; Jiang, Y.; Yang, D.; Cui, S. Effects of Different Mixture Ratios of Methanol-Diesel on the Performance Enhancement and Emission Reduction for a Diesel Engine. *Processes* **2021**, *9*, 1366. [[CrossRef](#)]

13. Yadav, J.; Ramesh, A. Injection strategies for reducing smoke and improving the performance of a butanol-diesel common rail dual fuel engine. *Appl. Energy* **2018**, *212*, 1–12. [[CrossRef](#)]
14. Cai, T.; Zhao, D.; Sun, Y.; Ni, S.; Li, W.; Guan, D.; Wang, B. Evaluation of NO_x emissions characteristics in a CO₂-Free micro-power system by implementing a perforated plate. *Renew. Sustain. Energy Rev.* **2021**, *145*, 111150. [[CrossRef](#)]
15. Delogu, M.; Del Pero, F.; Romoli, F.; Pierini, M. Life cycle assessment of a plastic air intake manifold. *Int. J. Life Cycle Assess.* **2015**, *20*, 1429–1443. [[CrossRef](#)]
16. Diéguez, P.M.; Urroz, J.C.; Sáinz, D.; Machin, J.; Arana, M.; Gandía, L.M. Characterization of combustion anomalies in a hydrogen-fueled 1.4 L commercial spark-ignition engine by means of in-cylinder pressure, block-engine vibration, and acoustic measurements. *Energy Convers. Manag.* **2018**, *172*, 67–80. [[CrossRef](#)]
17. Zhang, Z.; Ye, J.; Lv, J.; Xu, W.; Tan, D.; Jiang, F.; Huang, H. Investigation on the effects of non-uniform porosity catalyst on SCR characteristic based on the field synergy analysis. *J. Environ. Chem. Eng.* **2022**, *10*, 107056. [[CrossRef](#)]
18. Zhang, Z.; Tian, J.; Xie, G.; Li, J.; Xu, W.; Jiang, F.; Huang, Y.; Tan, D. Investigation on the combustion and emission characteristics of diesel engine fueled with diesel/methanol/n-butanol blends. *Fuel* **2022**, *314*, 123088. [[CrossRef](#)]
19. E, J.; Zhao, X.; Qiu, L.; Wei, K.; Zhang, Z.; Deng, Y.; Han, D.; Liu, G. Experimental investigation on performance and economy characteristics of a diesel engine with variable nozzle turbocharger and its application in urban bus. *Energy Convers. Manag.* **2019**, *193*, 149–161. [[CrossRef](#)]
20. Ebrahimi, R. A new design method for maximizing the work output of cycles in reciprocating internal combustion engines. *Energy Convers. Manag.* **2018**, *172*, 164–172. [[CrossRef](#)]
21. Polverino, P.; D’Aniello, F.; Arsie, I.; Pianese, C. Study of the energetic needs for the on-board production of Oxy-Hydrogen as fuel additive in internal combustion engines. *Energy Convers. Manag.* **2019**, *179*, 114–131. [[CrossRef](#)]
22. Xu, Z.; Fu, J.; Liu, J.; Yuan, Z.; Shu, J.; Tan, L. Comparison of in-cylinder combustion and heat-work conversion processes of vehicle engine under transient and steady-state conditions. *Energy Convers. Manag.* **2017**, *132*, 400–409. [[CrossRef](#)]
23. Wang, W.; Zuo, Z.; Liu, J. Miniaturization limitations of rotary internal combustion engines. *Energy Convers. Manag.* **2016**, *112*, 101–114. [[CrossRef](#)]
24. Yang, X.; Liao, C.; Liu, J. Harmonic analysis and optimization of the intake system of a gasoline engine using GT-power. *Energy Procedia* **2012**, *14*, 756–762. [[CrossRef](#)]
25. Qi, Y.; Dong, L.; Liu, H.; Puzinauskas, P.; Midkiff, K. Optimization of intake port design for SI engine. *Int. J. Automot. Technol.* **2012**, *13*, 861–872. [[CrossRef](#)]
26. Pai, D.; Singh, H.S.; Muhammed, F. Simulation Based Approach for Optimization of Intake Manifold. *SAE Tech. Pap.* **2011**. [[CrossRef](#)]
27. Silva, E.; Ochoa, A.; Henriquez, J. Analysis and runners length optimization of the intake manifold of a 4-cylinder spark ignition engine. *Energy Convers. Manag.* **2019**, *188*, 310–320. [[CrossRef](#)]
28. Zhang, Z.; E, J.; Chen, J.; Zhao, X.; Zhang, B.; Deng, Y.; Peng, Q.; Yin, Z. Effects of boiling heat transfer on the performance enhancement of a medium speed diesel engine fueled with diesel and rapeseed methyl ester. *Appl. Therm. Eng.* **2020**, *169*, 114984. [[CrossRef](#)]
29. Leahu, C.-I. Improvement of exhaust gas pressure’s utilization for compressing the intake air in diesel engine’s cylinders. *Int. J. Automot. Technol.* **2015**, *16*, 913–921. [[CrossRef](#)]
30. Wang, G.; Yu, W.; Li, X.; Yang, R. Influence of fuel injection and intake port on combustion characteristics of controllable intake swirl diesel engine. *Fuel* **2019**, *262*, 116548. [[CrossRef](#)]
31. Ma, B.; Yao, A.; Yao, C.; Wu, T.; Wang, B.; Gao, J.; Chao, C. Exergy loss analysis on diesel methanol dual fuel engine under different operating parameters. *Appl. Energy* **2020**, *261*, 114483. [[CrossRef](#)]
32. Kang, W.; Pyo, S.; Kim, H. Comparison of intake and exhaust throttling for diesel particulate filter active regeneration of non-road diesel engine with mechanical fuel injection pump. *Int. J. Engine Res.* **2020**, *22*, 146808742092603. [[CrossRef](#)]
33. Cheng, L.; Dimitriou, P.; Weiji, W.; Peng, J.; Aitouche, A. A novel fuzzy logic variable geometry turbocharger and exhaust gas recirculation control scheme for optimizing the performance and emissions of a diesel engine. *Int. J. Engine Res.* **2018**, *21*, 1298–1313. [[CrossRef](#)]
34. Li, Z.; Zhang, Y.; Huang, G.; Zhao, W.; He, Z.; Qian, Y.; Lu, X. Control of intake boundary conditions for enabling clean combustion in variable engine conditions under intelligent charge compression ignition (ICCI) mode. *Appl. Energy* **2020**, *274*, 115297. [[CrossRef](#)]
35. Song, K.; Upadhyay, D.; Xie, H. An assessment of the impacts of low-pressure exhaust gas recirculation on the air path of a diesel engine equipped with electrically assisted turbochargers. *Int. J. Engine Res.* **2019**, *22*, 1–19. [[CrossRef](#)]
36. Zhen, X.; Li, X.; Wang, Y.; Liu, D.; Tian, Z.; Wang, Y. Effects of the initial flame kernel radius and EGR rate on the performance, combustion and emission of high-compression spark-ignition methanol engine. *Fuel* **2019**, *262*, 116633. [[CrossRef](#)]
37. Arnau, F.; Martín, J.; Pla, B.; Auñón, Á. Diesel engine optimization and exhaust thermal management by means of variable valve train strategies. *Int. J. Engine Res.* **2020**, *22*, 146808741989480. [[CrossRef](#)]
38. E, J.; Zhiqing, Z.; Tu, Z.; Wei, Z.; Hu, W.; Han, D.; Jin, Y. Effect analysis on flow and boiling heat transfer performance of cooling water-jacket of bearing in the gasoline engine turbocharger. *Appl. Therm. Eng.* **2018**, *130*, 754–766. [[CrossRef](#)]
39. Zhang, Z.; E, J.; Deng, Y.; Pham, M.; Zuo, W.; Peng, Q.; Yin, Z. Effects of fatty acid methyl esters proportion on combustion and emission characteristics of a biodiesel fueled marine diesel engine. *Energy Convers. Manag.* **2018**, *159*, 244–253. [[CrossRef](#)]

40. Xia, M.; Zhang, F. Application of Multi-Parameter Fuzzy Optimization to Enhance Performance of a Regulated Two-Stage Turbocharged Diesel Engine Operating at High Altitude. *Energies* **2020**, *13*, 4278. [[CrossRef](#)]
41. Huang, R.; Dai, Y.; Luo, X.; Wang, Y.; Huang, C. Multi-objective optimization of the flush-type intake duct for a waterjet propulsion system. *Ocean Eng.* **2019**, *187*, 106172. [[CrossRef](#)]
42. Zhang, Z.; Li, J.; Tian, J.; Xie, G.; Tan, D.; Qin, B.; Huang, Y.; Cui, S. Effects of Different Diesel-Ethanol Dual Fuel Ratio on Performance and Emission Characteristics of Diesel Engine. *Processes* **2021**, *9*, 1135. [[CrossRef](#)]
43. Shang, Z.; Yu, X.; Shi, W.; Huang, S.; Li, G.; Guo, Z.; He, F. Numerical research on effect of hydrogen blending fractions on idling performance of an n-butanol ignition engine with hydrogen direct injection. *Fuel* **2019**, *258*, 116082. [[CrossRef](#)]
44. Jiang, F.; Li, M.; Wen, J.; Tan, Z.; Zhou, W. Optimization Analysis of Engine Intake System Based on Coupling Matlab-Simulink with GT-Power. *Math. Probl. Eng.* **2021**, *2021*, 6673612. [[CrossRef](#)]
45. Bancalari, E.; Diakunchak, I.; McQuiggan, G. A Review of W501G Engine Design, Development and Field Operating Experience. *ASME Pap.* **2003**, *GT2003-38956*, 963–969. [[CrossRef](#)]
46. Fahd, M.E.A.; Wenming, Y.; Lee, P.S.; Chou, S.K.; Yap, C.R. Experimental investigation of the performance and emission characteristics of direct injection diesel engine by water emulsion diesel under varying engine load condition. *Appl. Energy* **2013**, *102*, 1042–1049. [[CrossRef](#)]
47. Liu, T.; E, J.; Yang, W.; Hui, A.; Cai, H. Development of a skeletal mechanism for biodiesel blend surrogates with varying fatty acid methyl esters proportion. *Appl. Energy* **2016**, *162*, 278–288. [[CrossRef](#)]
48. E, J.; Liu, T.; Yang, W.M.; Deng, Y.; Gong, J. A skeletal mechanism modeling on soot emission characteristics for biodiesel surrogates with varying fatty acid methyl esters proportion. *Appl. Energy* **2016**, *181*, 322–331. [[CrossRef](#)]
49. Zuo, H.; Tan, J.; Wei, K.; Huang, Z.; Zhong, D.; Xie, F. Effects of different poses and wind speeds on wind-induced vibration characteristics of a dish solar concentrator system. *Renew. Energy* **2021**, *168*, 1308–1326. [[CrossRef](#)]
50. Zuo, H.; Liu, G.; E, J.; Zuo, W.; Wei, K.; Hu, W.; Tan, J.; Zhong, D. Catastrophic analysis on the stability of a large dish solar thermal power generation system with wind-induced vibration. *Sol. Energy* **2019**, *183*, 40–49. [[CrossRef](#)]
51. Zuo, H.; Zhang, B.; Huang, Z.; Wei, K.; Tan, J. Effect analysis on SOC values of the power lithium manganate battery during discharging process and its intelligent estimation. *Energy* **2022**, *238*, 121854. [[CrossRef](#)]
52. Xie, Y.; Zuo, Q.; Zhu, G.; Guan, Q.; Wei, K.; Zhang, B.; Tang, Y.; Shen, Z. Investigations on the soot combustion performance enhancement of an improved catalytic gasoline particulate filter regeneration system under different electric heating powers. *Fuel* **2021**, *283*, 119301. [[CrossRef](#)]
53. Chen, J.; Wang, Q.; Xu, Z.; E, J.; Leng, E.; Zhang, F.; Liao, G. Process in supercritical water gasification of coal: A review of fundamentals, mechanisms, catalysts and element transformation. *Energy Convers. Manag.* **2021**, *237*, 114122. [[CrossRef](#)]
54. Muhssen, H.S.; Masuri, S.U.; Bin Sahari, B.; Hairuddin, A.A. Design improvement of compressed natural gas (CNG)-Air mixer for diesel dual-fuel engines using computational fluid dynamics. *Energy* **2021**, *216*, 118957. [[CrossRef](#)]
55. Ning, L.; Duan, Q.; Zhanming, C.; Kou, H.; Liu, B.; Yang, B.; Zeng, K. A comparative study on the combustion and emissions of a non-road common rail diesel engine fueled with primary alcohol fuels (methanol, ethanol, and n-butanol)/diesel dual fuel. *Fuel* **2020**, *266*, 117034. [[CrossRef](#)]
56. E, J.; Liu, G.; Zhang, Z.; Han, D.; Chen, J.; Wei, K.; Gong, J.; Yin, Z. Effect analysis on cold starting performance enhancement of a diesel engine fueled with biodiesel fuel based on an improved thermodynamic model. *Appl. Energy* **2019**, *243*, 321–335. [[CrossRef](#)]
57. Chen, L.; Deng, Y.; Feng, C.; Han, W.; E, J.; Wang, C.; Han, D.; Zhang, B. Effects of zeolite molecular sieve on the hydrocarbon adsorbent performance of gasoline engine of during cold start. *Fuel* **2022**, *310*, 122427. [[CrossRef](#)]
58. E, J.; Luo, J.; Han, D.; Tan, Y.; Feng, C.; Deng, Y. Effects of different catalysts on light-off temperature of volatile organic components in the rotary diesel particulate filter during the regeneration. *Fuel* **2022**, *310*, 122451. [[CrossRef](#)]